

DPA: Learning Robust Physical Adversarial Camouflages for Object Detectors

Yixin Duan¹, Jialin Chen², Xingyu Zhou¹, Junhua Zou¹, Zhengyun He¹, Wu Zhang¹ and Zhisong Pan^{1*}

¹Army Engineering University of PLA, Nanjing, China

²The 28th Research Institute of China Electronics Technology Group Corporation, Nanjing, China

Abstract

Adversarial attacks are feasible in the real world for object detection. However, most of the previous works have tried to learn “patches” applied to an object to fool detectors, which become less effective or even ineffective in squint view angles. To address this issue, we propose the Dense Proposals Attack (DPA) to learn *robust, physical* and *targeted* adversarial camouflages for detectors. The camouflages are robust because they remain adversarial when filmed under arbitrary viewpoint and different illumination conditions, physical because they function well both in the 3D virtual scene and the real world, and targeted because they can cause detectors to misidentify an object as a specific target class. In order to make the generated camouflages robust in the physical world, we introduce a combination of viewpoint shifts, lighting and other natural transformations to model the physical phenomena. In addition, to improve the attacks, DPA substantially attacks all the classifications in the fixed region proposals. Moreover, we build a virtual 3D scene using the Unity simulation engine to fairly and reproducibly evaluate different physical attacks. Extensive experiments demonstrate that DPA outperforms the state-of-the-art methods significantly, and generalizes well to the real world, posing a potential threat to the security-critical computer vision systems.

1 Introduction

Deep neural networks (DNNs) have achieved remarkable performance on various visual recognition tasks [Simonyan and Zisserman, 2014; He *et al.*, 2016; Szegedy *et al.*, 2016; Ren *et al.*, 2015; Redmon and Farhadi, 2018]. Despite the great success, DNNs are found to be vulnerable to adversarial examples [Szegedy *et al.*, 2013], inputs with adversarial noises, which can fool the deep models without impeding human recognition. This leads to the study of attack and defense techniques for DNNs, and the adversarial attack for image tasks include image classification [Dong *et al.*, 2018;

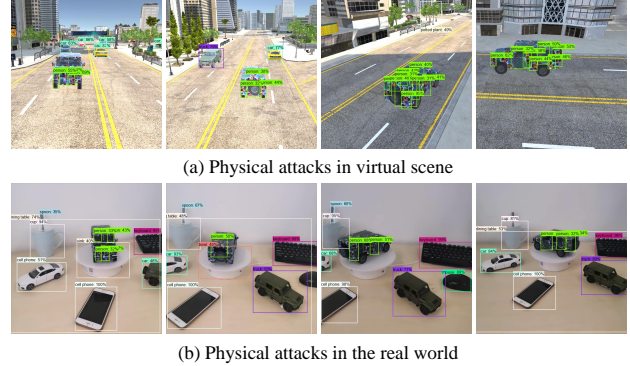


Figure 1: Physical attacks (DPA) against the Faster R-CNN detector in (a) 3D virtual scene and (b) real world in free viewpoints under different brightness conditions. The adversarial vehicles are detected as the target label (e.g., person). Zoom in for more details.

Xie *et al.*, 2019; Dong *et al.*, 2019], object detection [Xie *et al.*, 2017; Chen *et al.*, 2018; Huang *et al.*, 2020] and semantic segmentation [Xie *et al.*, 2017; Chen *et al.*, 2017], etc. It poses serious concerns in security-critical areas, such as medical diagnosis [Wu *et al.*, 2021] and autonomous driving [Sitawarin *et al.*, 2018].

Adversarial noises can be divided into two categories: 1) imperceptible noise, which is too subtle to be effective in a physical world due to the destructive environmental noise, view point changes and other transformations [Lu *et al.*, 2017]; 2) visible noise, which completely replaces some local area of the input image, is noticeable to human, and the resultant adversarial example remains adversarial in the physical world [Brown *et al.*, 2017]. Attacks can be classified by the type of outcome the adversary desires: 1) non-targeted attack, the adversary’s goal is to cause the deep model to predict any incorrect label, and the specific incorrect label does not matter; 2) targeted attack, the adversary aims to change the deep model’s prediction to the specific target class, which is more challenging [Liu *et al.*, 2016; Kurakin *et al.*, 2018].

In application domains, the attacks can be classified into digital attack and physical attack: 1) digital attack, which assumes that the attackers have “digital-level” access to an input, e.g., they can arbitrarily add adversarial noises to the in-

*Corresponding author

put images, which tends to be infeasible in real-world vision systems such as web cameras and autonomous vehicles [Song *et al.*, 2018]; 2) physical attack, which generates adversarial objects in the physical simulators or real world [Athalye *et al.*, 2018]. Some works generate small objects like 3D baseballs and turtles for image classifiers [Athalye *et al.*, 2018], which are adversarial within a small range of camera-to-object distances. However, it is significantly harder to attack object detectors than classifiers, as it needs to mislead the classification results in multiple bounding boxes with different scales [Chen *et al.*, 2018].

Previous works have investigated the vulnerability of object detectors to adversarial objects in physical world. However, there are several limitations: 1) the adversarial noises are only for planar or view-restricted objects, such as adversarial patches and stop signs [Song *et al.*, 2018; Chen *et al.*, 2018; Thys *et al.*, 2019; Huang *et al.*, 2020; Wang *et al.*, 2021], which would be less effective for the object with arbitrary view angle in the real world; 2) misidentifying the adversarial object as any incorrect class, not as a specific target class [Zhang *et al.*, 2019], (e.g., for autonomous driving, misidentifying an object as a designated traffic light or person is more threatening than randomly misidentifying it as a cake); 3) the missing of a unified physical evaluation environment makes it difficult to fairly compare and evaluate the experimental results of different attacks [Huang *et al.*, 2020]. To address these issues, we extend these works to generate robust, physical and targeted adversarial objects, and build a simulation scene based on the Unity¹ engine for evaluation.

In this paper, we propose the Dense Proposals Attack (DPA) method to generate a 3D vehicle with the full-painted adversarial camouflage. The generated adversarial camouflage can mislead detectors to identify the vehicle as a specific target class from any view angle, which can evaluate the robustness of the DNN-based detectors more accurately. To synthesize the robust 3D adversarial vehicle, we choose a distribution of environment conditions to render various poses of the 3D adversarial vehicle as well as lighting and other natural transformations. In addition, inspired by the data augmentation strategy in adversarial attacks, which optimizes an adversarial example with a set of transformed (e.g., translated, resized) images, and has been proven effective to prevent the adversarial examples from overfitting to the white-box model being attacked [Xie *et al.*, 2019; Dong *et al.*, 2019], DPA attacks all the classifications in the fixed dense proposals of Faster R-CNN [Ren *et al.*, 2015] to improve the transferability of the adversarial objects.

To fairly evaluate the effectiveness of different physical attacks, we use the Unity simulation engine to build a photo-realistic 3D urban scene with high fidelity streets, buildings, plants, billboard, etc. The simulation engine enables us to conduct experiments under a variety of environmental conditions: lighting, backgrounds, camera-to-object distances, view angles, occlusions, etc. Experimental results demonstrate that the vehicle with full-painted camouflage can be consistently misidentified as the target class by the detectors in arbitrary viewpoint. Figure 1 shows some sampled result

images in the simulation virtual scene and the real world.

In summary, our main contributions are as following:

- To the best of our knowledge, our work is the first to learn 3D full-painted object camouflages which can consistently fool object detectors to output a designated target label.
- The proposed DPA optimizes the adversarial objects with dense proposals, which alleviates the overfitting phenomenon, and obtains adversarial objects with strong transferability.
- We build a Unity simulation scene to fairly and reproducibly evaluate the effectiveness of different attacks.
- The proposed DPA achieves state-of-the-art results for attacking object detectors and is well generalized to the real world.

2 Related Works

2.1 Digital Attacks

Digital attacks generate adversarial noises for inputs in the digital pixel domain. A series of attack methods [Szegedy *et al.*, 2013; Goodfellow *et al.*, 2014; Kurakin *et al.*, 2016a; Carlini and Wagner, 2017; Dong *et al.*, 2018; Xie *et al.*, 2019; Dong *et al.*, 2019] have been proposed to generate adversarial examples to attack the image classifiers. Xie et al. [2017] extended adversarial examples from image classification to object detection, and generate visually imperceptible perturbations to fool detectors. Although these attacks work well in the digital world, they become significantly less effective when introduced into the physical world [Lu *et al.*, 2017].

2.2 Physical Attacks

Physical attacks usually add visible local noises to the input so that the generated adversarial examples remain adversarial in the physical world. Brown et al. [2017] generated robust adversarial patches in the real world, which caused the image classifiers to ignore the other items in the scene and report a chosen target class. Eykholt et al. [2018] targeted the task of stop sign classification, and caused misclassification by applying sticker perturbations. Athalye et al. [2018] optimized the expectation over the transformation by applying different modifications when generating adversarial examples, and obtained robust 3D adversarial examples for image classification.

The more challenging physical attacks on object detection have also been studied. Chen et al. [2018] generated adversarial perturbed stop signs to fool detectors. Song et al. [2018] used synthetic transformations to attack object detection models, causing the object detectors ignore the stop sign with sticker perturbations. Thys et al. [2019] and Huang et al. [2020] learned adversarial patterns to attack instances belonging to the same object category. Wang et al. [2021] generated visually-natural physical adversarial patches, which can suppress both model and human attention. However, all of the adversarial patterns generated by these works are viewpoint-limited, and the attack effect drops off sharply as the viewpoint shifts. Zhang et al. [2019] learned camouflages to make a vehicle randomly misidentified as other classes, such as a

¹<https://unity.com>

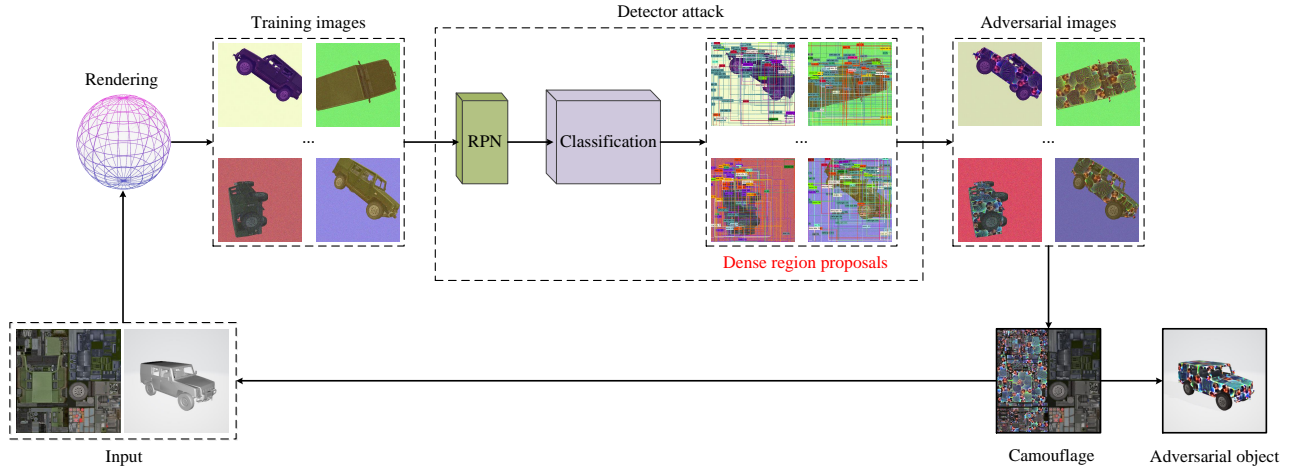


Figure 2: Overview of the pipeline to generate the adversarial camouflage. 1) Input transformation. The camouflage is mapped to a rendering of the vehicle, and according to a given distribution, the transformations include viewpoint shifts, lighting, backgrounds, and camera noises to obtain the physical training images. 2) Detector attack. We simultaneously attack all the classifications in the fixed dense region proposals, and update the camouflage perturbations by minimizing the cross-entropy losses. Zoom in for more details.

cake or even a boat. On the contrast, we aim to make vehicles be consistently misidentified as specific classes that closely related to traffic safety, such as person, which would be more threatening and challenging.

3 Methodology

In this section, we first introduce the overview of pipeline to generate the adversarial camouflage, then provide the detailed description of our method.

3.1 Overview

Our goal is to generate camouflages which can fool the object detectors to misidentify a vehicle as the target class or hide the vehicle from being detected under different viewing and lighting conditions.

Although projective transformations could be used to render the planar objects into a variety of images, it is more involved for the non-planar 3D objects in this paper. We train the adversarial objects in physical space, rather than in 2D space that the resulting objects being adversarial only from restricted viewpoints.

We simultaneously model both the object perspectives and the physical environment variations, so as to generate adversarial object that is robust from any viewpoint. To deal with the complex operation, similar to [Athalye *et al.*, 2018], the transformation functions map the camouflage to a rendering of the vehicle, simulating functions including rotation, translation, perspective projection as well as lighting, background changing and environmental noise.

Next, we attack the Faster R-CNN model [Ren *et al.*, 2015], a two-stage detector, under the white-box setting. We first run the region proposal network (RPN), and prune the region proposals by non-maximum suppression (NMS). Then we fix the top- n (e.g., 300) pruned region proposals and feed them to the second stage classification, and

attack all the classifications in these proposals simultaneously to generates robust camouflages [Ren *et al.*, 2015; Chen *et al.*, 2018]. As illustrated in Figure 2, DPA mainly consists of two steps:

- Step 1. Obtaining the training images on-the-fly by simulating the 3D geometrical transformations as well as the physical environment variations.
- Step 2. Attacking all the classifications in the fixed dense region proposals simultaneously.

3.2 3D Rendering

Let (\mathbf{m}, \mathbf{c}) be a 3D object with a mesh tensor \mathbf{m} and a texture tensor \mathbf{c} . The training image x with ground-truth label y is the rendered result of the 3D object (\mathbf{m}, \mathbf{c}) with different environment conditions $e \in \mathbf{E}$ (e.g., view angles, camera-to-object distances, lighting, noises, backgrounds, etc, the distribution detailed in Table 3 in the Appendix) from a renderer \mathcal{R} by

$$x = \mathcal{R}((\mathbf{m}, \mathbf{c}), e) \quad (1)$$

To perform physical attacks to fool a detector $f(\cdot)$, we obtain adversarial camouflage texture \mathbf{c}_{adv} by adding perturbations to the original \mathbf{c} , and generate the adversarial example as

$$x_{adv} = \mathcal{R}((\mathbf{m}, \mathbf{c}_{adv}), e) \quad (2)$$

where $(\mathbf{m}, \mathbf{c}_{adv})$ is the obtained 3D adversarial object.

3.3 Dense Proposals Attack

For the non-targeted attack, an adversarial example is to make the deep model output a wrong prediction, which can be expressed as $f(x_{adv}) \neq y$; for the targeted attack, it aims to fool the deep model into outputting a specific target label y^* , which can be express as $f(x_{adv}) = y^*$, and $y^* \neq y$. In this paper, we focus on the more challenging targeted attack.

The Faster R-CNN is a two-stage model. The region proposal network (RPN) in the first stage is a fully convolutional network that simultaneously predicts object bounds and

scores at each position. The classifier in the second stage performs classification in each region proposal. Each detection includes a probability distribution over K pre-defined classes as well as the location of the detected object.

For the targeted attack, the objective is to minimize the cross-entropy loss function $J(f(x_{adv}), y^*)$ of the classifier. We do not constrain the distance between the \mathbf{c}_{adv} and the original \mathbf{c} , because for three-dimensional objects, it hardly impedes human recognition. Therefore, the optimization problem for attacking the classification of an object in one proposal can be written as

$$\arg \min_{\mathbf{c}_{adv}} J(f(x_{adv}), y^*) \quad (3)$$

Convolutional neural networks are supposed to be approximately invariant to translation, rotation and other transformations [LeCun *et al.*, 1995; Cohen and Welling, 2016], that an object in the input can be recognized in spite of its position or angle. It has been found that using a set of transformed images to optimize an adversarial example can improve the transferability significantly [Dong *et al.*, 2019; Xie *et al.*, 2019], which is proposed for image classification. This data augmentation strategy alleviates overfitting in adversarial attacks, thus making the generated adversarial examples more transferable [Xie *et al.*, 2019]. We extend the strategy to the object detection task.

Some RPN proposals highly overlap with each other. To reduce redundancy, most model adopt non-maximum suppression (NMS) to prune the proposal regions based on their confidence scores [Ren *et al.*, 2015]. To improve the attacks, in each iteration, we first run the region proposal network, then fix the pruned proposals after NMS. The label of each proposal is defined as the corresponding confident class. In the second classification stage, we minimize the cross-entropy losses between the target class and the predicted classes in all the fixed dense proposals. Similar to data augmentation, the objects in the fixed region proposals can be regarded as a set of transformed (e.g., translated, cropped) sub-images, which can alleviate the overfitting problem and improve the transferability of the generated adversarial objects. We refer the proposed method as Dense Proposals Attack (DPA), and find it produced a good solution.

Let n be the number of the fixed proposals, and the output of each image is $\mathcal{P} = \{p_i | p_i = (s_i, b_i); i = 1, 2, 3 \dots n\}$, where s_i is the confidence score and b_i represents the location of the i -th region proposal. In order to enhance the attack, rather than optimize the objective function at a single point as Eq. (3), DPA simultaneously attacks the classifications of all the fixed dense region proposals to optimize the adversarial camouflage as

$$\arg \min_{\mathbf{c}_{adv}} \left[\frac{1}{n} \sum_{p_i \in \mathcal{P}} J(f(x_{adv}, p_i), y^*) \right] \quad (4)$$

Therefore, the camouflage is trained to optimize the object function

$$\arg \min_{\mathbf{c}_{adv}} \mathbb{E}_{x \sim \mathbf{X}, e \sim \mathbf{E}} \left[\frac{1}{n} \sum_{p_i \in \mathcal{P}} J(f(x_{adv}, p_i), y^*) \right] \quad (5)$$

Algorithm 1 Algorithm of DPA

Input: 3D object (\mathbf{m}, \mathbf{c}) , environment condition parameter $e \in \mathbf{E}$, neural renderer \mathcal{R} , target class label y^* , detector f , maximal iteration number N .
Output: Adversarial camouflage tensor \mathbf{c}_{adv} .

- 1: $\mathbf{c}_{adv}^0 \leftarrow \mathbf{c}$;
- 2: **for** $t = 0$ to $N - 1$ **do**
- 3: Generate training images in each iteration:
 $x_{adv}^t \leftarrow \mathcal{R}((\mathbf{m}, \mathbf{c}_{adv}^t), e)$
- 4: Obtain the dense region proposals:
 $\mathcal{P} = \{p_i | p_i = (s_i, b_i); i = 1, 2, 3 \dots n\}$;
- 5: Update \mathbf{c}_{adv}^t via attacking all the classifications of the proposals:

$$\arg \min_{\mathbf{c}_{adv}^t} \mathbb{E}_{x \sim \mathbf{X}, e \sim \mathbf{E}} \left[\frac{1}{n} \sum_{p_i \in \mathcal{P}} J(f(x_{adv}^t, p_i), y^*) \right],$$

$$\mathbf{c}_{adv}^t = \text{Clip}(\mathbf{c}_{adv}^t, 0, 1);$$
- 6: **end for**
- 7: **return:** $\mathbf{c}_{adv} = \mathbf{c}_{adv}^N$.

where \mathbf{X} is the training set of images generated by the renderer, \mathbf{E} is the distribution of the environment conditions simulated by the renderer, and \mathbb{E} is the Expectation over Transformation (EOT) technique [Athalye *et al.*, 2018] which models the adversarial perturbations within the optimization procedure. The “true” input $\mathcal{R}((\mathbf{m}, \mathbf{c}_{adv}), e)$ perceived by the detector $f(\cdot)$ is the input object $(\mathbf{m}, \mathbf{c}_{adv})$ with environment condition e after render operations. It optimizes the losses between the expected detection results and the target class y^* . The resultant camouflage pixel value is clipped to the valid range (i.e., $[0, 1]$ for images). The overall procedure of DPA is illustrated in Algorithm 1.

4 Experiments

In this section, we conduct extensive experiments to demonstrate the effectiveness of the proposed method. First we specify the experimental settings, then we introduce the simulation scene used for testing, and finally we evaluate the proposed method based on the experimental results. We restrict the camouflage to the body of the vehicle, leaving tires, windows, lightings, etc. unaltered as the discriminative visual cues for the detectors.

4.1 Experimental Settings

Source Model. We generate adversarial camouflage on the Faster R-CNN with Inception-v2 [Szegedy *et al.*, 2016] as the backbone network. The model is trained on the Microsoft Common Objects in Context (COCO2014) dataset [Lin *et al.*, 2014], which contains 80 general object classes. We denote this model as FR-Incv2-14. Faster R-CNN is one of the state-of-the-art general object detector, which adopts a two-stage detection strategy. The first stage generates many region proposals that may contain objects, and the second stage outputs the classification results and the refined bounding box coordinates.

Target Models. We test the results both on the two-stage and one-stage detectors for validating the transferability of the adversarial camouflage generated by the source model.

For two-stage detectors, we evaluate the performance of Faster R-CNN model, in addition to Inception-v2, the backbone networks include VGG16 [Simonyan and Zisserman, 2014] and ResNet-101 [He *et al.*, 2016], which are either trained on the PascalVOC-2007 trainval set, or the combined PascalVOC-2007 and PascalVOC-2012 trainval set [Everingham *et al.*, 2015]. We denote these models as FR-VGG16-07, FR-RES101-07, FR-VGG-0712 and FR-RES101-0712. For one-stage detectors, we select YOLOv3 model [Redmon and Farhadi, 2018], whose network structure is quite different from Faster R-CNN, making it challenging to carry out transfer attacks to it, we denote this model trained on COCO2014 dataset as YOLOv3-14.

Evaluation Metrics. The principal quantitative measure of detection task is the average precision (AP). Detections are considered true or false positives based on the area Intersection over Union (IoU) between the predicted box B_p and the ground truth box B_{gt} , which is defined as $IoU = \frac{B_p \cap B_{gt}}{B_p \cup B_{gt}}$. The threshold of IoU is set to 0.5 as in the PASCAL VOC detection challenge [Everingham *et al.*, 2015] to determine whether the detector hits or misses the true category. This metrics is denoted as P@0.5 [Zhang *et al.*, 2019; Huang *et al.*, 2020]. The confidence score threshold of all models is set to 0.3 for evaluation. (Since the jeep vehicle with the original texture is detected as a truck or a car, we consider both classes to be “true” classes).

Baselines. We generate some simple textures for comparison, *Natural*, *Naive* and *Random*, as shown in Figure 3. In addition, we compare our method to several state-of-the-art works on the 3D physical attacks. Adversarial patches [Thys *et al.*, 2019], which generate adversarial patches to fool a detector by minimizing different probabilities related to the appearance of a object, and this method is denoted as *AdvPat*. Shapeshifter [Chen *et al.*, 2018] obtains adversarial objects that mislead a detector via EOT technique, and this method is denoted as *Shape*. *UPC* [Huang *et al.*, 2020] crafts effective adversarial camouflages for non-rigid or non-planar objects. *Camou* [Zhang *et al.*, 2019] learns camouflages that can hide a vehicle from detectors.

4.2 Physical Simulation

To fairly evaluate different attacks, we use the Unity engine to build a photo-realistic 3D simulation scene, which is controllable and reproducible.

Virtual Scene. The virtual scene is a typical urban environment (shown in Figure 7 in the Appendix), with architectures, traffic signs, streets, etc. We demonstrate attack results with a high-fidelity 3D vehicle. The simulation engine enables us to conduct experiments under different environmental conditions: view angles, camera-to-object distances, lighting, backgrounds, occlusions, etc.

Camera Setting. Cameras are located around the vehicle. As illustrated in Figure 4 (a), the view angles and distances of the cameras distribute freely as free viewpoints within a semi-ellipsoid, so that the attack effect can be evaluated more accurately and comprehensively.

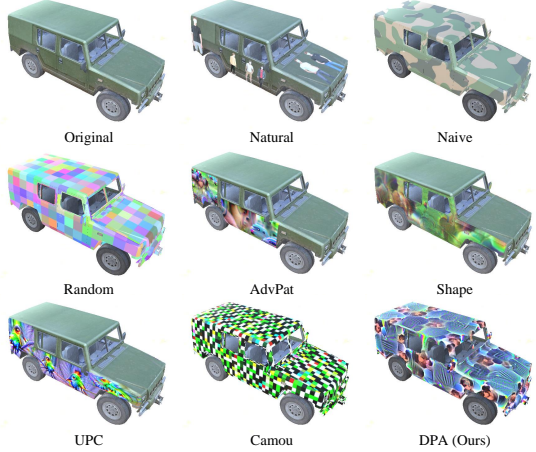


Figure 3: Examples of different vehicle textures. **Original**: vehicle with the original texture; **Natural**: vehicle with natural images as camouflage patterns; **Naive**: vehicle with simple army camouflage; **Random**: vehicle with random mosaic camouflage; **Advpat**, **Shape**, **UPC** and **Camou** are vehicles with adversarial patterns generated by the baseline methods; **DPA**: vehicle with the adversarial camouflage generated by the proposed DPA.

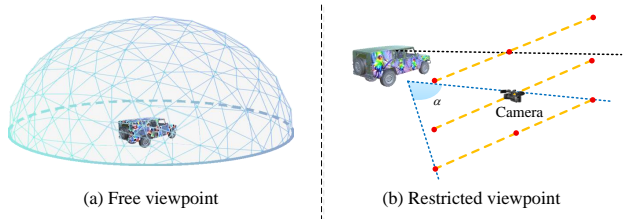


Figure 4: The camera settings. (a) The camera is placed arbitrarily within a semi-ellipsoid as free viewpoints; (b) the camera is limited to a certain view angle (e.g., *UPC* with restricted view angle α).

Illumination Setting. Previous works usually conduct tests in bright environments. However, there are a lot of dark scenes in the real world. Therefore, we extend the testing environment to better evaluate the effectiveness of the camouflage. The area light and directional light sources are used to get 2 levels brightness (i.e., bright: L_b and dark: L_d) simulation scenes (illustrated in Figure 1 (a)).

4.3 Virtual Scene Experiments

Firstly, we conduct comparison experiments with simple textures to demonstrate that the successful attack is not due to the domain gap between the real data used to train the detectors and the simulation data, and evaluate the transferability of the adversarial camouflage generated by DPA under different illumination conditions. Secondly, we compare the proposed DPA with several existing physical attack methods under different viewpoint settings.

As illustrated in Figure 3, nine different vehicle textures are used for comprehensive experimental comparison to evaluate the effectiveness of the proposed DPA. 400 (200×2) images with free viewpoints in different locations of the simulation scene are rendered for each of the nine vehicles.

| Model | FR-Incv2-14 | | | FR-VGG16-07 | | | FR-VGG16-0712 | | | FR-RES101-07 | | | FR-RES101-0712 | | | YOLOv3-14 | | |
|----------|-------------|-------|----------------------|-------------|-------|----------------------|---------------|-------|----------------------|--------------|-------|----------------------|----------------|-------|----------------------|-----------|-------|----------------------|
| | L_b | L_d | Avg (Drop) | L_b | L_d | Avg (Drop) | L_b | L_d | Avg (Drop) | L_b | L_d | Avg (Drop) | L_b | L_d | Avg (Drop) | L_b | L_d | Avg (Drop) |
| Original | 1.00 | 1.00 | 1.00 (-) | 0.91 | 0.96 | 0.94 (-) | 0.96 | 0.97 | 0.97 (-) | 0.98 | 0.99 | 0.98 (-) | 0.99 | 0.96 | 0.97 (-) | 1.00 | 1.00 | 1.00 (-) |
| Natural | 1.00 | 1.00 | 1.00 (0) | 0.89 | 0.92 | 0.90 (0.04) | 0.91 | 0.94 | 0.93 (0.04) | 0.95 | 0.99 | 0.97 (0.01) | 0.93 | 0.95 | 0.94 (0.03) | 0.94 | 0.90 | 0.92 (0.08) |
| Naive | 1.00 | 0.94 | 0.97 (0.03) | 0.94 | 0.75 | 0.84 (0.10) | 0.96 | 0.84 | 0.90 (0.07) | 0.93 | 0.90 | 0.91 (0.07) | 0.90 | 0.94 | 0.92 (0.05) | 0.92 | 0.82 | 0.87 (0.13) |
| Random | 0.92 | 0.96 | 0.94 (0.06) | 0.87 | 0.74 | 0.81 (0.13) | 0.94 | 0.92 | 0.93 (0.04) | 0.89 | 0.90 | 0.90 (0.08) | 0.99 | 0.94 | 0.96 (0.01) | 0.81 | 0.63 | 0.72 (0.28) |
| DPA | 0.14* | 0.06* | 0.10 (0.90) | 0.20 | 0.11 | 0.16 (0.78) | 0.33 | 0.25 | 0.29 (0.68) | 0.61 | 0.56 | 0.58 (0.40) | 0.75 | 0.81 | 0.78 (0.19) | 0.17 | 0.21 | 0.19 (0.81) |

Table 1: Average precision P@0.5 and drop rates in virtual scene experiments under two illumination level settings. Each P@0.5 is averaged over free viewpoints. * indicates the white-box attacks. The best results are in bold.

| Model | FR-Incv2-14 | | | FR-VGG16-07 | | | FR-VGG16-0712 | | | FR-RES101-07 | | | FR-RES101-0712 | | | YOLOv3-14 | | |
|----------|-----------------------|-----------------------|----------------------|----------------------|-----------------------|----------------------|----------------------|----------------------|-------------|----------------------|----------------------|----------------------|----------------------|----------------------|----------------------|----------------------|--|--|
| | RV (Drop) | FV (Drop) | RV (Drop) | FV (Drop) | RV (Drop) | FV (Drop) | RV (Drop) | FV (Drop) | RV (Drop) | FV (Drop) | RV (Drop) | FV (Drop) | RV (Drop) | FV (Drop) | RV (Drop) | FV (Drop) | | |
| Original | 1.00 (-) | 1.00 (-) | 1.00 (-) | 0.94 (-) | 1.00 (-) | 0.97 (-) | 1.00 (-) | 0.97 (-) | 1.00 (-) | 0.98 (-) | 1.00 (-) | 0.97 (-) | 1.00 (-) | 0.97 (-) | 1.00 (-) | 1.00 (-) | | |
| AdvPat | 0.90 (0.10) | 0.95 (0.05) | 0.54 (0.46) | 0.75 (0.19) | 0.48 (0.52) | 0.72 (0.25) | 0.81 (0.19) | 0.89 (0.09) | 0.91 (0.09) | 0.93 (0.04) | 0.16* (0.84) | 0.50* (0.50) | 0.90 (0.10) | 0.89 (0.11) | 0.90 (0.10) | 0.89 (0.11) | | |
| Shape | 0.99* (0.01) | 0.98* (0.02) | 0.90 (0.10) | 0.90 (0.04) | 0.87 (0.13) | 0.87 (0.10) | 0.98 (0.02) | 0.95 (0.03) | 0.99 (0.01) | 0.95 (0.02) | 0.59 (0.41) | 0.68 (0.32) | 0.65 (0.35) | 0.80 (0.17) | 0.55* (0.45) | 0.30* (0.70) | | |
| UPC | 0.97 (0.03) | 0.99 (0.01) | 0.18 (0.82) | 0.55 (0.39) | 0.09* (0.91) | 0.51* (0.46) | 0.73 (0.27) | 0.84 (0.14) | 0.65 (0.35) | 0.80 (0.17) | 0.99 (0.01) | 0.95 (0.02) | 0.55* (0.45) | 0.30* (0.70) | 0.12 (0.88) | 0.19 (0.81) | | |
| Camou | 0.96 (0.04) | 0.69 (0.31) | 0.89 (0.11) | 0.77 (0.17) | 0.92 (0.08) | 0.75 (0.22) | 0.99 (0.01) | 0.91 (0.07) | 0.99 (0.01) | 0.95 (0.02) | 0.55* (0.45) | 0.30* (0.70) | 0.71 (0.29) | 0.78 (0.19) | 0.12 (0.88) | 0.19 (0.81) | | |
| DPA | 0.09* (0.91) | 0.10* (0.90) | 0.10 (0.90) | 0.16 (0.78) | 0.23 (0.77) | 0.29 (0.68) | 0.51 (0.49) | 0.58 (0.40) | 0.71 (0.29) | 0.78 (0.19) | 0.12 (0.88) | 0.19 (0.81) | 0.12 (0.88) | 0.19 (0.81) | 0.12 (0.88) | 0.19 (0.81) | | |

Table 2: Average precision P@0.5 and drop rates of different attacks in restricted and free viewpoints. Each P@0.5 is averaged over two brightness levels. * indicates the white-box attacks. The best results are in bold.

Comparison with Simple Textures. We use three simple textures (*Natural*, *Naive* and *Random*) as well as the original texture for comparison. For autonomous driving systems, “person” is more important and appears more frequently than other categories such as “cake” and “bird”, so we choose “person” as the target class to fool the detectors in the experiments.

The results of average precision are shown in Table 1. We can find that for the *Natural*/*Naive*/*Random* textures, the average precisions of almost all models drop little, indicating that simple textures hardly affect the detectors, i.e., the detectors are robust to the simulation data. On the contrast, the camouflage generated by DPA significantly reduces the average precisions under both the bright and dark brightness conditions, verifying the effectiveness of the attack.

In addition, we can observe that for the simple textures and the adversarial texture, most of the attacks in the dark environment are stronger than those in the bright environment, which may be attributed to the fact that the robustness of the detector is relatively weak when the brightness level is low, resulting in an easier reduction of average precision.

Further, we evaluate the cross-model and cross-training transferability. The average precision of the “Original” texture in Table 1 is used as the baseline precision for each model. FR-Incv2-14 is the source model used for training the adversarial camouflage. The target models include FR-VGG16-07, FR-VGG16-0712, FR-RES101-07, FR-RES101-0712 and YOLOv3-14, the first four models are two-stage detection models and the last one is a one-stage detection model. All models are publicly available.

For the cross-model transferability, we compare the average precision of the source model and the target models which have different network structures. We can see that the average precisions of DPA on YOLOv3-14 drop significantly, indicating that the resultant camouflage is highly transferable.

For FR-VGG16-07, FR-VGG16-0712, FR-RES101-07 and FR-RES101-0712 with both the model structures and training data sets different from the source model, it can be seen that DPA can also significantly reduce the average precisions. The average drop rates of the VGG16 based and the

ResNet101 based models are about 0.73 and 0.30, respectively. The drop rates of ResNet101 based models decrease less than other models, possibly because the ResNet101 network is deeper and has skip connections, which makes the network structure more distinct from the source model and more difficult to attack.

Comparison with Existing Attacks. We compare DPA with existing physical attacks on object detection. As can be seen in Figure 3, except for *Camou*, the adversarial patterns of *AdvPat*, *Shape* and *UPC* are on the sides of the vehicle. We denote the side view as *Restricted Viewpoint (RV)* (shown in Figure 4 (b), α is set to 120° , i.e., the left and right view angles are within 60°). However, the surveillance cameras do not film the vehicle object only from the side, the surround *Free Viewpoint (FV)* (shown in Figure 4 (a)) is more realistic, which can evaluate the attack effect of the adversarial patterns more accurately.

Table 2 shows the physical attack results of different methods under the restricted viewpoint and free viewpoint settings, respectively. It can be seen that for the attacks with adversarial patterns on the sides of the vehicle, the average precision in free viewpoints are significantly higher than that in restricted viewpoints (i.e., lower drop rates), and the attack effect becomes worse. For example, the average precision of *AdvPat* against YOLOv3-14 changed from 0.16 to 0.50, and that of *UPC* against FR-VGG16-0712 changed from 0.09 to 0.51. That is because when the view angle deviates from the side of the vehicle, the side patterns will be deformed, resulting in the attack effect decreased or even invalid.

We observe that the *Shape* works worse than other baselines. We speculate the reason is that *Shape* causes the resulting adversarial pattern itself to be misdetected (such as an adversarially perturbed stop sign), rather than suppressing the detection of the object covered by the pattern.

We can also find that the attacks of *Camou* which with a mosaic-like full painted camouflage are more effective in free views than in restricted views, e.g., the average precision of *Camou* against YOLOv3-14 is reduced from 0.55 to 0.30. This might be that in other viewpoints, the camouflage disrupts more discriminative features of the vehicle, making it

more likely to be misdetected.

Our adversarial camouflage achieves significantly better performance, and the drop rates in free viewpoints are much higher than all baseline methods. A noteworthy comment is that *Camou* is trained on YOLOv3-14 and DPA is trained on FR-Incv2-14, but the drop rates of DPA against YOLOv3-14 are significantly higher than that of *Camou*, which further demonstrates the cross-model transferability of DPA. Moreover, *Camou* is a non-targeted attack, while DPA is a targeted attack, which is more challenging.

We find that the specific target class can also be transferred, i.e., the target models also misidentify the vehicles with our adversarial camouflage trained on the source model FR-Incv2-14 as the person class label. This is because different models have similar decision boundaries due to the similar or same training dataset [Xie *et al.*, 2019]. See Figure 8, 9, 10 and 11 in the Appendix for more details.

4.4 Physical Environment Experiment

We evaluate physical attacks in the real world over a 3D-printed vehicle with the full painted camouflage generated by DPA. The unperturbed vehicles can be correctly detected as the true class over a large number of samples. During the physical experiments, we take photos and record videos with an HONOR 20 cell phone. Similar to the virtual scene experiments, the 3D-printed vehicle is filmed in free viewpoints. We put the vehicle on a rotating turntable, and the phone camera moves left and right to get as many views as possible. Figure 1 (b) shows some sampled images, and a demo video can be found at: <https://www.bilibili.com/video/BV1zL411J73r>.

In Figure 5 we plot the relationship between camera-to-object distance and the average precision of FR-Incv2-14. The abscissa is the ratio of distance to the vehicle length. It can be seen that the precisions increase as the distance increases. This is probably because the camouflage captured with lower quality from a distance. The results show low detection precisions, which demonstrate that the 3D-printed adversarial vehicle is strongly adversarial over a variety of viewpoints, and the camouflage generated by the virtual scene experiments exhibits high generalization to the real world.

4.5 Model Attention Analysis

In this part, we adopt model attention visualization to conduct qualitative analysis to further validate the effectiveness of our DPA attack.

The regions that the models pay attention to can be deemed as the discriminative regions. We generate the attention maps of the vehicle with different viewpoints on VGG16 model by the model-agnostic Grad-CAM technique [Selvaraju *et al.*, 2017]. Figure 6 shows the original vehicle, virtual adversarial vehicle (Virtual-Adv), 3D printed adversarial vehicle (Real-Adv) and their attention maps for the “jeep” class label, respectively. We can observe the DPA attack distracts the the attention maps from the vehicle body to other uncamouflaged regions.

5 Conclusion

In this paper, we investigate the problem of generating robust adversarial examples in the physical world for object detec-

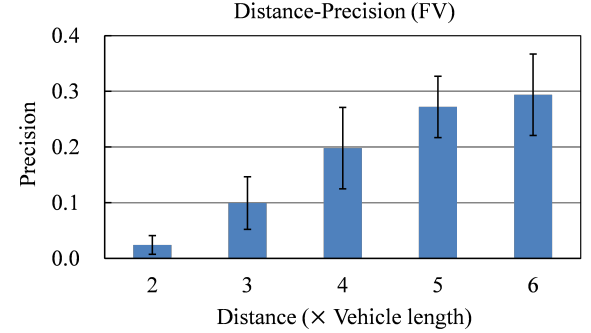


Figure 5: Average precisions (with $\pm \text{std}$ over 5 tests) of detection under different distance conditions in the real world.

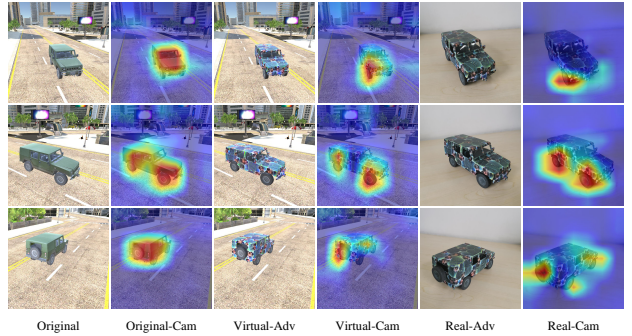


Figure 6: Visualization of discriminative regions for “jeep” class label in the virtual scene and the real world. For the vehicles with the adversarial camouflage, the model places its attention predominantly on the regions with no adversarial perturbations (e.g., tires).

tors. By modeling the 3D rendering, and using a set of dense proposals to optimize the adversarial camouflage in each iteration, the vehicle with the resultant adversarial camouflage generated by the proposed DPA exhibits significantly better performance than the state-of-the-art baseline methods. In addition, we build a 3D scene to evaluate different attacks fairly and reproducibly. With the 3D printing technology, we successfully fabricate a physical adversarial vehicle that is detected as a specific target class in a variety of viewpoints and lighting conditions, demonstrating the effectiveness of the proposed method.

References

- [Athalye *et al.*, 2018] Anish Athalye, Logan Engstrom, Andrew Ilyas, and Kevin Kwok. Synthesizing robust adversarial examples. In *International conference on machine learning*, pages 284–293. PMLR, 2018.
- [Brown *et al.*, 2017] Tom B Brown, Dandelion Mané, Aurko Roy, Martín Abadi, and Justin Gilmer. Adversarial patch. *arXiv preprint arXiv:1712.09665*, 2017.
- [Carlini and Wagner, 2017] Nicholas Carlini and David Wagner. Towards evaluating the robustness of neural networks. In *2017 IEEE Symposium on Security and Privacy (SP)*, pages 39–57. IEEE, 2017.

- [Chen *et al.*, 2017] Liang-Chieh Chen, George Papandreou, Florian Schroff, and Hartwig Adam. Rethinking atrous convolution for semantic image segmentation. *arXiv preprint arXiv:1706.05587*, 2017.
- [Chen *et al.*, 2018] Shang-Tse Chen, Cory Cornelius, Jason Martin, and Duen Horng Polo Chau. Shapeshifter: Robust physical adversarial attack on faster r-cnn object detector. In *Joint European Conference on Machine Learning and Knowledge Discovery in Databases*, pages 52–68. Springer, 2018.
- [Cohen and Welling, 2016] Taco Cohen and Max Welling. Group equivariant convolutional networks. In *International conference on machine learning*, pages 2990–2999. PMLR, 2016.
- [Dong *et al.*, 2018] Yinpeng Dong, Fangzhou Liao, Tianyu Pang, Hang Su, Jun Zhu, Xiaolin Hu, and Jianguo Li. Boosting adversarial attacks with momentum. In *Proceedings of the IEEE conference on computer vision and pattern recognition*, pages 9185–9193, 2018.
- [Dong *et al.*, 2019] Yinpeng Dong, Tianyu Pang, Hang Su, and Jun Zhu. Evading defenses to transferable adversarial examples by translation-invariant attacks. In *Proceedings of the IEEE Conference on Computer Vision and Pattern Recognition*, pages 4312–4321, 2019.
- [Everingham *et al.*, 2015] Mark Everingham, SM Ali Eslami, Luc Van Gool, Christopher KI Williams, John Winn, and Andrew Zisserman. The pascal visual object classes challenge: A retrospective. *International journal of computer vision*, 111(1):98–136, 2015.
- [Eykholt *et al.*, 2018] Kevin Eykholt, Ivan Evtimov, Earlene Fernandes, Bo Li, Amir Rahmati, Chaowei Xiao, Atul Prakash, Tadayoshi Kohno, and Dawn Song. Robust physical-world attacks on deep learning visual classification. In *Proceedings of the IEEE conference on computer vision and pattern recognition*, pages 1625–1634, 2018.
- [Goodfellow *et al.*, 2014] Ian J Goodfellow, Jonathon Shlens, and Christian Szegedy. Explaining and harnessing adversarial examples. *arXiv preprint arXiv:1412.6572*, 2014.
- [He *et al.*, 2016] Kaiming He, Xiangyu Zhang, Shaoqing Ren, and Jian Sun. Deep residual learning for image recognition. In *Proceedings of the IEEE conference on computer vision and pattern recognition*, pages 770–778, 2016.
- [Huang *et al.*, 2020] Lifeng Huang, Chengying Gao, Yuyin Zhou, Cihang Xie, Alan L Yuille, Changqing Zou, and Ning Liu. Universal physical camouflage attacks on object detectors. In *Proceedings of the IEEE/CVF Conference on Computer Vision and Pattern Recognition*, pages 720–729, 2020.
- [Kurakin *et al.*, 2016a] Alexey Kurakin, Ian Goodfellow, and Samy Bengio. Adversarial examples in the physical world. *arXiv preprint arXiv:1607.02533*, 2016a.
- [Kurakin *et al.*, 2018] Alexey Kurakin, Ian Goodfellow, Samy Bengio, Yinpeng Dong, Fangzhou Liao, Ming Liang, Tianyu Pang, Jun Zhu, Xiaolin Hu, Cihang Xie, et al. Adversarial attacks and defences competition. In *The NIPS’17 Competition: Building Intelligent Systems*, pages 195–231. Springer, 2018.
- [LeCun *et al.*, 1995] Yann LeCun, Yoshua Bengio, et al. Convolutional networks for images, speech, and time series. *The handbook of brain theory and neural networks*, 3361(10):1995, 1995.
- [Lin *et al.*, 2014] Tsung-Yi Lin, Michael Maire, Serge Belongie, James Hays, Pietro Perona, Deva Ramanan, Piotr Dollár, and C Lawrence Zitnick. Microsoft coco: Common objects in context. In *European conference on computer vision*, pages 740–755. Springer, 2014.
- [Liu *et al.*, 2016] Yanpei Liu, Xinyun Chen, Chang Liu, and Dawn Song. Delving into transferable adversarial examples and black-box attacks. *arXiv preprint arXiv:1611.02770*, 2016.
- [Lu *et al.*, 2017] Jiajun Lu, Hussein Sibai, Evan Fabry, and David Forsyth. No need to worry about adversarial examples in object detection in autonomous vehicles. *arXiv preprint arXiv:1707.03501*, 2017.
- [Redmon and Farhadi, 2018] Joseph Redmon and Ali Farhadi. Yolov3: An incremental improvement. *arXiv preprint arXiv:1804.02767*, 2018.
- [Ren *et al.*, 2015] Shaoqing Ren, Kaiming He, Ross Girshick, and Jian Sun. Faster r-cnn: Towards real-time object detection with region proposal networks. *Advances in neural information processing systems*, 28:91–99, 2015.
- [Selvaraju *et al.*, 2017] Ramprasaath R Selvaraju, Michael Cogswell, Abhishek Das, Ramakrishna Vedantam, Devi Parikh, and Dhruv Batra. Grad-cam: Visual explanations from deep networks via gradient-based localization. In *Proceedings of the IEEE international conference on computer vision*, pages 618–626, 2017.
- [Simonyan and Zisserman, 2014] Karen Simonyan and Andrew Zisserman. Very deep convolutional networks for large-scale image recognition. *arXiv preprint arXiv:1409.1556*, 2014.
- [Sitawarin *et al.*, 2018] Chawin Sitawarin, Arjun Nitin Bhagoji, Arsalan Mosenia, Mung Chiang, and Prateek Mittal. Darts: Deceiving autonomous cars with toxic signs. *arXiv preprint arXiv:1802.06430*, 2018.
- [Song *et al.*, 2018] Dawn Song, Kevin Eykholt, Ivan Evtimov, Earlene Fernandes, Bo Li, Amir Rahmati, Florian Tramer, Atul Prakash, and Tadayoshi Kohno. Physical adversarial examples for object detectors. In *12th {USENIX} Workshop on Offensive Technologies ({WOOT} 18)*, 2018.
- [Szegedy *et al.*, 2013] Christian Szegedy, Wojciech Zaremba, Ilya Sutskever, Joan Bruna, Dumitru Erhan, Ian Goodfellow, and Rob Fergus. Intriguing properties of neural networks. *arXiv preprint arXiv:1312.6199*, 2013.
- [Szegedy *et al.*, 2016] Christian Szegedy, Vincent Vanhoucke, Sergey Ioffe, Jon Shlens, and Zbigniew Wojna. Rethinking the inception architecture for computer vision. In *Proceedings of the IEEE conference on computer vision and pattern recognition*, pages 2818–2826, 2016.

[Thys *et al.*, 2019] Simen Thys, Wiebe Van Ranst, and Toon Goedemé. Fooling automated surveillance cameras: adversarial patches to attack person detection. In *Proceedings of the IEEE/CVF Conference on Computer Vision and Pattern Recognition Workshops*, pages 0–0, 2019.

[Wang *et al.*, 2021] Jiakai Wang, Aishan Liu, Zixin Yin, Shunchang Liu, Shiyu Tang, and Xianglong Liu. Dual attention suppression attack: Generate adversarial camouflage in physical world. In *Proceedings of the IEEE/CVF Conference on Computer Vision and Pattern Recognition*, pages 8565–8574, 2021.

[Wu *et al.*, 2021] Yu-Huan Wu, Shang-Hua Gao, Jie Mei, Jun Xu, Deng-Ping Fan, Rong-Guo Zhang, and Ming-Ming Cheng. Jcs: An explainable covid-19 diagnosis system by joint classification and segmentation. *IEEE Transactions on Image Processing*, 30:3113–3126, 2021.

[Xie *et al.*, 2017] Cihang Xie, Jianyu Wang, Zhishuai Zhang, Yuyin Zhou, Lingxi Xie, and Alan Yuille. Adversarial examples for semantic segmentation and object detection. In *Proceedings of the IEEE International Conference on Computer Vision*, pages 1369–1378, 2017.

[Xie *et al.*, 2019] Cihang Xie, Zhishuai Zhang, Yuyin Zhou, Song Bai, Jianyu Wang, Zhou Ren, and Alan L Yuille. Improving transferability of adversarial examples with input diversity. In *Proceedings of the IEEE Conference on Computer Vision and Pattern Recognition*, pages 2730–2739, 2019.

[Zhang *et al.*, 2019] Yang Zhang, Hassan Foroosh, Philip David, and Boqing Gong. Camou: Learning physical vehicle camouflages to adversarially attack detectors in the wild. In *International Conference on Learning Representations*, 2019.

Appendix

A Environment Condition

Table 3 shows the distribution of environment condition parameters we chosen.

| Environment condition | Minimum | Maximum |
|-----------------------------------|---------------|---------------|
| Camera distance | 1.5 | 6.0 |
| X/Y translation | -0.05 | 0.05 |
| Rotation | any | |
| Background | (0.1,0.1,0.1) | (1.0,1.0,1.0) |
| Lighten / Darken (additive) | -0.15 | 0.15 |
| Lighten / Darken (multiplicative) | 0.5 | 2.0 |
| Per-channel (additive) | -0.15 | 0.15 |
| Per-channel (multiplicative) | 0.7 | 1.3 |
| Gaussian Noise (stdev) | 0.0 | 0.1 |

Table 3: Distribution of environment condition parameters for the physical world, approximating rendering, physical-world phenomena, and printing error.

B Virtual Scene

Figure 7 shows some locations of the virtual scene.



Figure 7: An urban scene built for evaluating the attacks.

C 3D Adversarial Objects

Figure 8, 9, 10 and 11 show the detection results of different models for the vehicles with camouflages generated by different methods under different viewing and lighting conditions. Figure 12 shows two adversarial vehicles with other target class camouflages generated by DPA.

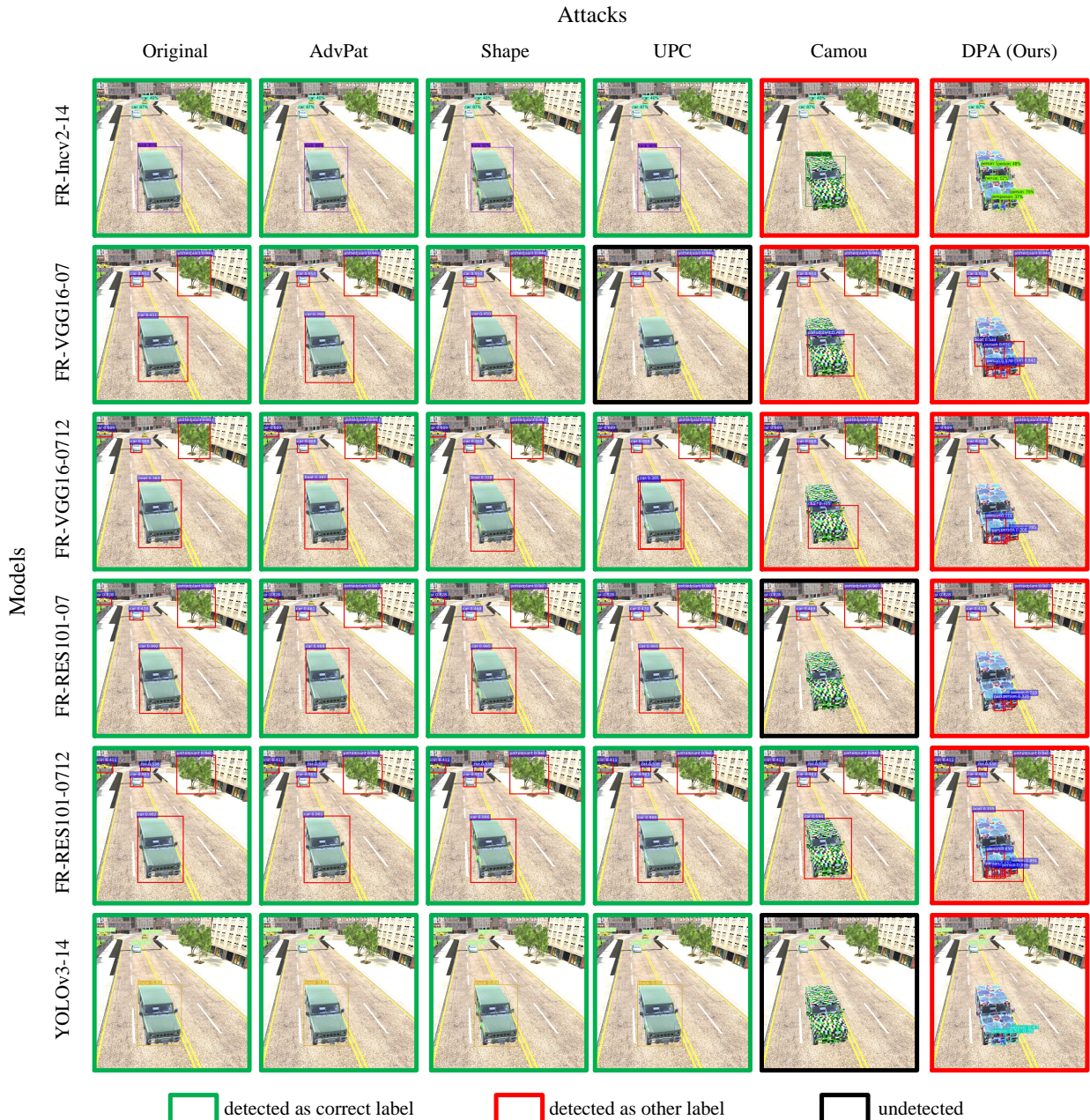


Figure 8: A sample of the 3D adversarial vehicles under the bright environment condition.

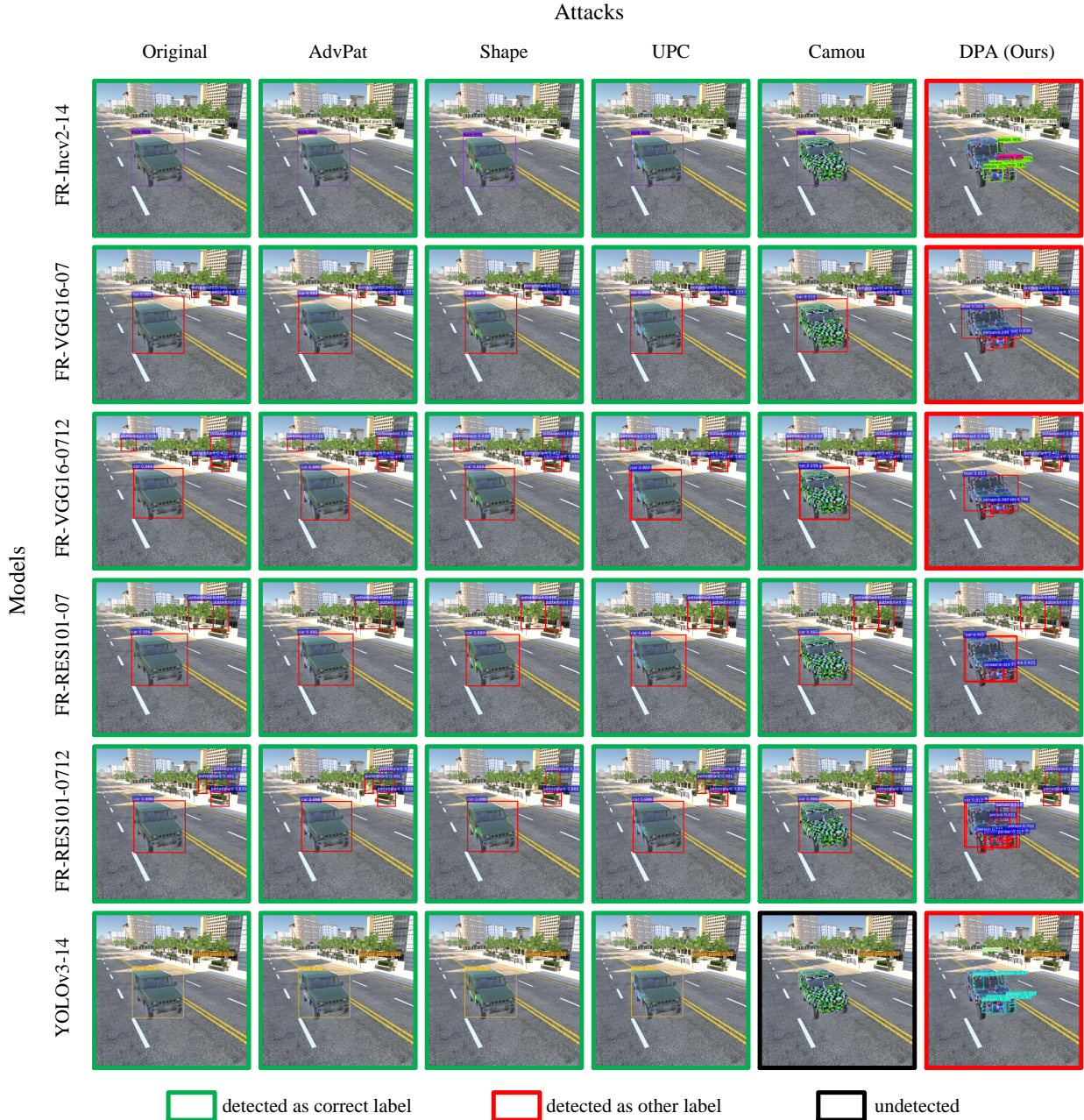


Figure 9: A sample of the 3D adversarial vehicles under the dark environment condition.

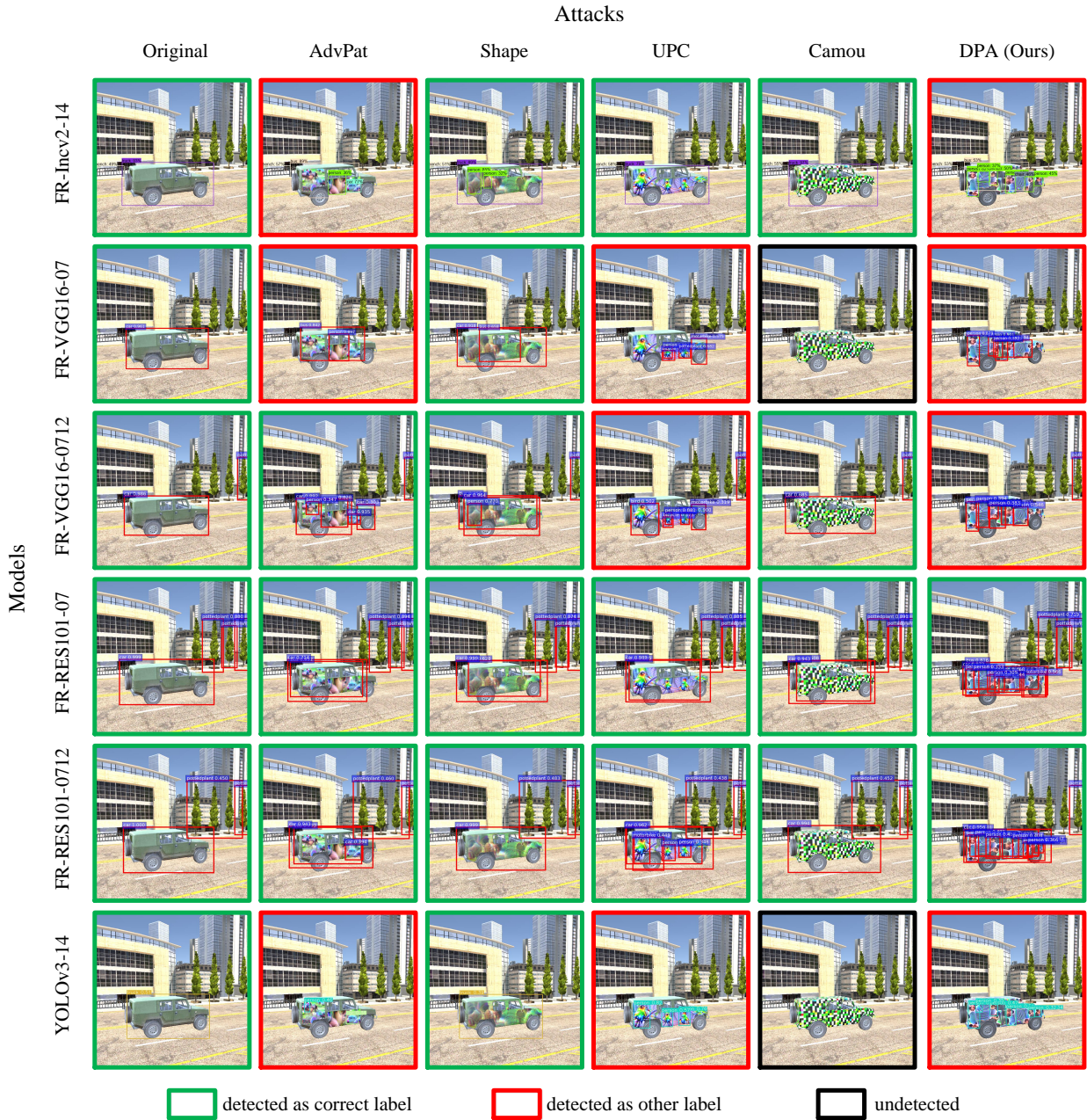


Figure 10: A sample of the 3D adversarial vehicles under the bright environment condition.

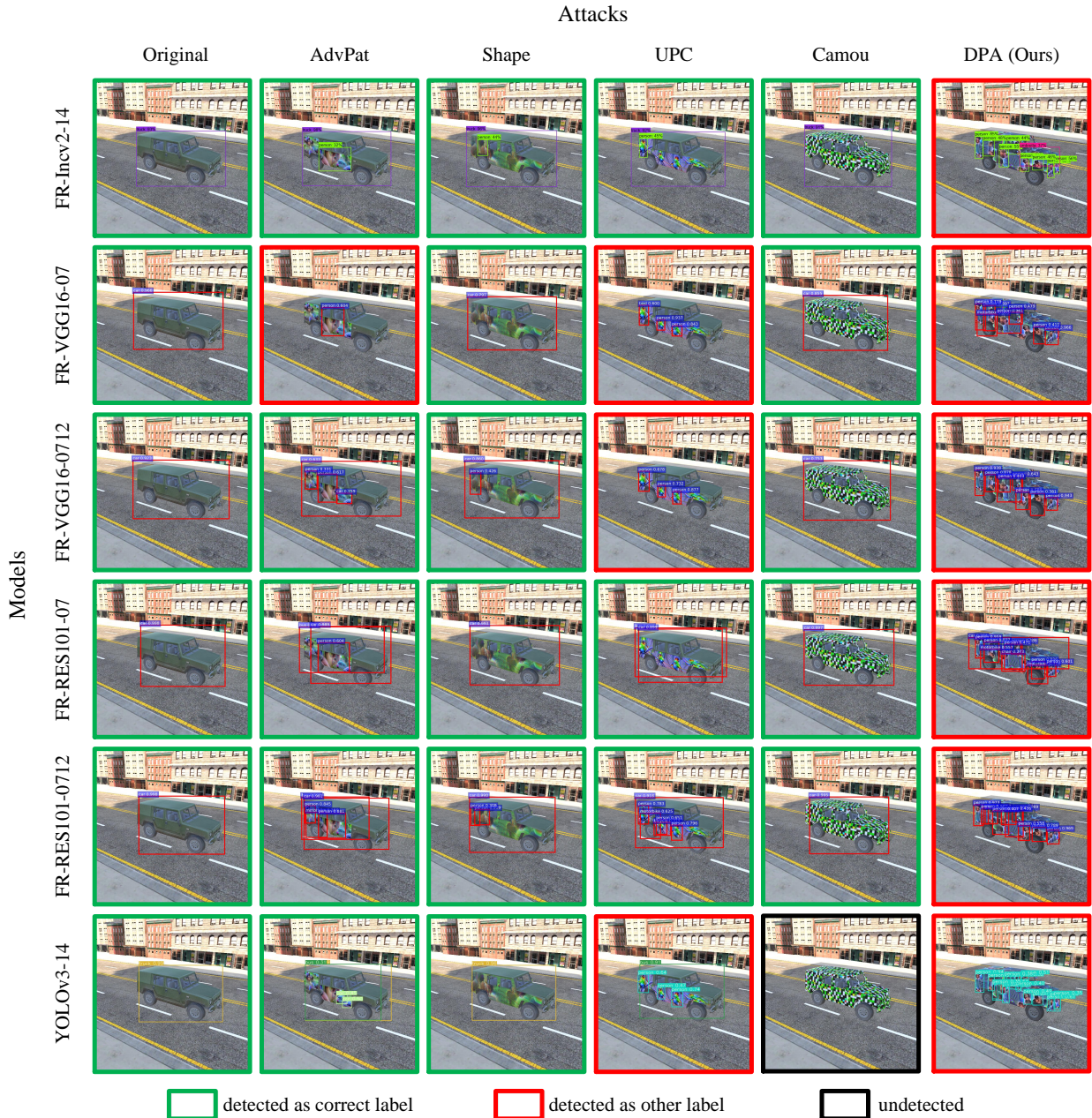
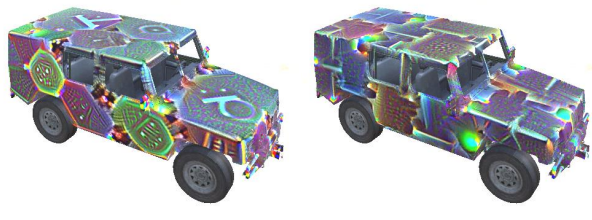


Figure 11: A sample of the 3D adversarial vehicles under the dark environment condition.



Target class: stop sign

Target class: traffic light

Figure 12: Adversarial vehicles with other target class camouflages generated by DPA.